International Journal of Thin Films Science and Technology

http://dx.doi.org/10.18576/ijtfst/100306

Efficient and Recyclable Cu Incorporated TiO_2 Nanoparticle Catalyst for Organic Dye Photodegradation

Anita Sagadevan Ethiraj [1,*], *Danielle S. Rhen* [2], *Alexander V. Soldatov* [3], *Gomaa A. M. Ali* [4] *and Zinab H. Bakr* [5]

[1] Department of Physics, VIT-AP University, Amaravati, Andhra Pradesh 522237, India
[2] School of Material Science and Engineering, Tiangong University, Tianjin, 300387, P. R. China
[3] The Smart Materials Research Institute, Southern Federal University, Sladkova Str. 178/24, Rostov-on-Don, Russian Federation
[4] Chemistry Department, Faculty of Science, Al-Azhar University, Assiut 71524, Egypt
[5] Physics Department, Faculty of Science, Assiut University, Assiut 71516, Egypt

Received: 5 June 2021, Revised: 10 July 2021, Accepted: 18 July 2021.
Published online: 1 Sep. 2021.

Abstract: Highly efficient Cu-doped TiO_2 photocatalysts (CTO) with variation in Cu concentration (4 to 16 wt.%) were prepared via a modified sol-gel technique. X-ray diffraction (XRD) data indicate a pure anatase structure with a small crystallite size of 22.16 nm obtained for CTO-12 (12 wt.% Cu). The average crystallite size and energy bandgap with variation in Cu doping were also studied. All the samples exhibited a spherical morphology. The increment in the Cu concentration caused a systematic decrease in the photoluminescence (PL) intensity, which indicated a lower recombination rate of electron-hole pairs and hence higher separation efficiency. CTO-12 served as the best-suited photocatalyst, tested for photocatalytic degradation of cationic basic (methylene blue, rhodamine B) and anionic acidic (Methyl orange) dyes under UV light irradiation. The comparative study illustrates higher degradation efficiency obtained for cationic dyes than anionic dyes in the order of RhB>MB>MO. The highest degradation (95.3%) was obtained for RhB dye in 180 min. In addition, the further kinetic study suggested the degradation of dyes followed the first-order kinetics. The recyclability data demonstrated superior stability and reliability of the photocatalyst, suggesting its future utilization in potential wastewater treatment applications.

Keywords: Cu-doped TiO_2, Nanocatalyst, Photocatalysis, Photoluminescence, Photodegradation, Recycling.

1 Introduction

Titanium dioxide (TiO_2) is a potential material system utilized in photocatalysis to decompose organic pollutants present in air or water [1-4]. This is due to its exceptional properties, such as strong oxidizing ability, high stability in an aqueous environment, nontoxic nature, low cost, etc. [2, 5, 6]. The anatase phase formed at a lower temperature with an indirect optical bandgap around ~3.2-3.4 eV is mostly used for photodegradation, while the rutile phase finds its application pigment material [7-10]. However, solar and indoor light utilization is inefficient in TiO_2 due to its wide bandgap of about 3.2 eV [8, 11-13]. The possible solution to this problem is either narrowing the bandgap or creating separate energy states in the bandgap, thereby increasing light absorption capability. Doping is one way to modulate the host material lattice's optical, luminescent, physical, and magnetic properties. In semiconductors, doping also has an important impact on the nucleation and growth of many functional nanocrystals and modifies the size, morphology, crystallographic phase, and electronic configuration of nanomaterial [14-18]. Among all the transition metals, a narrow bandgap, and high absorption coefficient material, copper is widely used as a dopant for TiO_2 [19].

Choudhury et al. synthesized Cu-doped TiO_2 nanoparticles (NPs) (mixed-phase) by a sol-gel method from titanium tetra-isopropoxide (TTIP) and copper nitrate hexahydrate as precursors. They claimed that d states of Cu^{2+} and oxygen defects were responsible for narrowing the bandgap of TiO_2, which is responsible for increasing the magnitude of Urbach energy with Cu loading from 2 to 6% [8]. Other groups performed the linear and non-linear optical study of bare and Cu-doped TiO_2, also prepared via a sol-gel route where the anatase phase survived even after calcination at 500 °C [20]. The photodegradation of rhodamine B (RhB), congo red (CR), and methylene blue (MB) using 33 nm sized anatase TiO_2 prepared [21] was studied using sunlight. The study

*Corresponding author E-mail: ethirajanita25@gmail.com

was extended using wastewater after photocatalysis to examine the platelet interaction activity, MTT assay, and hemolysis effect. Another report illustrated improved (4-times) photocatalytic activity of MB dye using rutile mixed anatase TiO_2 nanosheets with dominant facets prepared via hydrothermal method compared to commercial P_{25} and anatase TiO_2 [22]. Kuyumcu et al. reported on the comparative studies performed for a series of transition metals, i.e., Cr, Mn, Fe, Co, Ni, and Cu-doped TiO_2 samples decolorizing methyl orange (MO) and MB dyes. Amongst all, the highest photocatalytic activity was observed for Cu (0.3 wt.%)/TiO_2 under visible light irradiation [23]. Recently the effect of various metals such as Cu, Ag, and Eu doped TiO_2 was tested for photocatalytic activity of organic dye under Xe as a light source [24]. Cu-doped anatase TiO_2 (8-12 nm) for the visible light photocatalytic antibacterial activity is also reported [8].

Cu-doped TiO_2 thin films in photodegradation studies are well documented in the literature [25, 26]. Zhang et al. reported Cu-doped thin films on Ag substrates for MB degradation experiments where an optimal thickness of 30 nm. Ag substrate improved the photocatalytic properties of TiO_2 with efficiency, reaching about 86% in 300 min under visible light [27]. On the contrary, Bensouici et al. studied the photocatalytic properties of films on a glass substrate with the same dye, which revealed a decrease in MB degradation concerning Cu concentration increase [28].

To achieve the high performance of Cu-doped TiO_2 materials, few groups emphasized the process of co-doping. Photodegradation of MO and MB dyes using the spheroid (Cu, N) co-doped TiO_2 (9-17 nm) photocatalysts via a microwave-assisted sol-gel method was recently prepared [29]. Other than textile dyes, photodegradation of toluene using Cu and V doped TiO_2 under UV and sunlight irradiation also exists [30]. Hamadanian et al. worked on the enhancement of photocatalysis of TiO_2 with the preparation of novel nanocomposites of metal (Co and Cu), nonmetal (C, N, S) doped TiO_2 photocatalyst [31]. Reports are also available for Cu-N co-doped TiO_2 NPs for MB dye, p nitrophenol decolorization, and Cu-N co-doped activated carbon (AC)/TiO_2 for photodegradation formaldehyde [32]. Transition metals doped TiO_2 nanofibers for the photodegradation of MO dyes tested under visible and UV irradiation were performed for photocatalytic hydrogen production [33]. Few nanohybrids based on Cu and TiO_2 NPs were also utilized for photodegradation of MO and RhB dyes [34-37].

Although reports are available on the application of TiO_2, doped TiO_2, TiO_2 composites in the photodegradation of various dyes, not much work has been reported on the application of Cu-doped TiO_2 nanoparticles photodegradation of organic dyes. This study's main objectives were to synthesize the pure anatase phase of Cu-doped TiO_2 NPs using a modified sol-gel technique and understand the relationship between the bandgap, average crystallite size, and variation Cu doping. Further photodegradation of cationic and anionic dyes subjected to UV light performed to investigate the performance of the best suited CTO nanocatalyst in photocatalysis.

2 Experimental Section

2.1 Synthesis of Cu-doped TiO_2 NPs

CTO was prepared by a sol-gel process, as reported elsewhere [20]. We slightly modified the synthesis process in this work, and all the precursors procured from Sigma Aldrich, i.e., TTIP, copper acetate, and 2-propanol, were used without further purification. In a typical procedure, 90 mL of extra pure 2-propanol was taken in a beaker, and 10 mL of aqueous solutions of cupric acetate with different concentrations (4, 8, 12, and 16 wt.% Cu) was added dropwise with vigorous stirring for 15 min. Later 10 mL of TTIP was incorporated into this solution and stirred vigorously for 45 min to obtain a homogeneous solution. The precipitate was obtained after centrifugation, then washed and dried at 80 °C for 5 h to evaporate the water and organic material. The dried powder was annealed at 500 °C for 5 h to produce the Cu-doped TiO_2 nanoparticles (CTO), pulverized to a powder using an agate mortar for further characterizations. The samples with Cu concentrations of 4, 8, 12, and 16 wt. % Cu used in the reactions were coded as CTO-4, CTO-8, CTO-12, and CTO-16, respectively.

2.2 Characterizations

X-ray diffraction (XRD) measurements of the CTO samples were performed using Philips PW-1710 diffractometer with Cu-Kα radiation (λ=1.540598 Å). UV-Vis spectroscopy was done by UV-VIS spectrophotometer Analytikjenaspecord 210 plus from 200-750 nm range. Diffuse reflectance data was measured by V-670 JAASCO equipment. Photoluminescence (PL) spectra were recorded using F-4500 spectrophotometer with 150 W xenon lamp in the wavelength range of 300-700 nm with 240 nm as excitation wavelength. Atomic Absorption Spectroscopy (AAS) was used to identify the copper concentration in the synthesized Cu-TiO2 NPs. The samples' external surface features and elemental analysis were recorded using Scanning Electron Microscope (SEM; FEI Quanta FEG 200–High-Resolution Scanning Electron Microscope) coupled with Energy-dispersive X-ray Spectroscopy (EDS).

2.3 Photodecolourization activity

In the present study, toxic effluent, mostly found in industrial textile wastewater, was chosen. MO served as an anionic dye, while MB and RhB dyes were selected as model cationic dyes. A 64 W, mercury vapor lamp was used as UV light source to activate the photocatalytic reactions. 10 mg of

catalysts were added to the 50 mL of aqueous dye solutions (10 mg/L) of MO, MB, and RhB. The mixture solution was stirred for 30 min inside the photoreactor chamber without light. This adsorption-desorption equilibrium in the dark was considered as zero time reading. The suspended solution was then subjected to UV light irradiation. The photodegradation of different dyes was studied by examining the dye concentration and decolorization. After every 15 min time interval, 5 mL of sample solution was taken out, centrifuged, and the sample dye solution's concentration was measured by UV-Vis absorbance spectrophotometer. Degradation percentage (%) was calculated using Eq. (1) [38-41].

$$Degradation\ (\%) = \frac{C_0 - C}{C_0} x100 \qquad (1)$$

Where C_o and C represent the concentrations of dye at time 0 and t, respectively.

3 Results and Discussion

X-ray diffraction patterns of CTO-4, CTO-8, CTO-12, and CTO-16 are displayed in Fig. 1a. The predominant (101), (004), (200) planes corresponding to 2θ values of 25.32, 37.71, 47.91° indicate pure anatase structure. Other peaks centered at 53.93, 55.06, 62.68, 68.69, 70.33, and 75.07° correspond to (105), (211), (204), (116), (220), and (215) planes match with the JCPDS card no. (21-1272). Even for Cu-TiO_2 thin films calcined at 500 °C the anatase TiO_2 phase was confirmed from the (101) plane obtained at 2θ of 25.33° [25]. Moreover, XRD data did not reveal the formation of impurities or any crystalline phase of copper species; hence it may be concluded that Cu ions are uniformly dispersed among the anatase TiO_2 crystallites.

The average crystallite size of the synthesized CTO samples as estimated utilizing the Debye Scherrer equation was found to be about 23.18, 24.29, 22.16, and 23.82 nm for CTO-4, CTO-8, CTO-12, and CTO-16, respectively. The bare TiO_2 sample showed a crystallite size of 23.00 nm, which indicates an increase in the crystallite size at the initial stage of Cu doping up to 8 wt.%. For Cu doping of 12 wt.%, size decreased, and with further increase in dopant concentration to 16 wt.%, it increased again. The smallest crystallite size was obtained for CTO-12 sample, i.e., 12 wt.% Cu doping. There is no systematic increase or decrease in crystallite size with variation in Cu doping, as observed by Rajamannan group [20]. Their results indicated the systematic increase in the crystallite size with variation in the concentration of Cu dopant. Moreover, the crystallite size was also not much affected by variation in Cu doping from 4 wt.% to 16 wt%, as reported by Bensouici et al. [28] for Cu-doped TiO_2 thin films.

The full width at half maximum (FWHM) of (101) plane endowed with a clue of strain concerning doped samples and decrease of crystallite size attributes to monotonically broadening of FWHM, which was noticed in Table 1. The calculated microstrain is also listed in Table 1. The CTO-12 sample with a minimum crystallite size of 22.16 nm exhibited a maximum strain of 0.4088, which is well in accordance with the literature reports. The suppression of crystalline size in CTO-12 sample attributes to the proper substitution of Cu^{2+} instead of Ti^{4+}, which will lead to distortion in the lattice; thus, more strain was observed in the smaller NPs. A similar trend of the relation between crystallite size, FWHM, and microstrain was observed in the published results of Anbuselvan and Muthukumuran [42], for Ni-doped ZnO and Ni, Cu co-doped ZnO samples. UV-Vis spectra of all CTO samples Fig. 1b showed a noticeably increased absorption towards the visible light region. CTO-4, CTO-8, CTO-12, and CTO-16 exhibited a single broad, intense peak at 261.97, 317.05, 268.70, and 283.76 nm. Compared to CTO-4, the absorbance peak is red-shifted for CTO-8, CTO-12, and CTO-16 samples. Redshift arises mainly due to a modification of TiO_2 with different concentrations of Cu. Reda et al. reported the redshift in the optical reflection edge for Cu-doped TiO_2, N-doped TiO_2, and Cu, N-codoped TiO_2, prepared via double technique including sol-gel [29]. Also, similar to these absorption results, redshift was reported for different Pd doping concentrations (0.05, 0.1, and 0.3%) in TiO_2 NPs [43]. Further, CTO-12 and CTO-16 exhibited a blue shift due to the quantum confinement effect compared to CTO-8 sample. Moreover, the AAS technique confirmed Cu's presence in all samples with an estimated weight percentage of Cu dopant in the TiO_2 NP as CTO-4:0.75 wt.%, CTO-8:1.93 wt.%, CTO-12:3.77 wt.%, CTO-16:5.21 wt.%, respectively. We were interested in incorporating about 5 wt.% Cu in TiO_2 nanoparticles; therefore, we increased the amount of Cu doping percent during the reaction synthesis up to 16% and were successful in doping - 5.21 wt.% in TiO_2 nanoparticles.

Bandgap measurements of CTO samples were done by analyzing the reflectance data. Photon energy (hυ) and absorption coefficient (α) are related to each other by Tauc equation (Eq. 2) [44-49]. Here, n represents the type of transition, E_g the optical bandgap, and C is a constant, depending on the transition probability.

$$ahv = C(h\upsilon - E_g)^n \qquad (2)$$

Here, in this case, anatase TiO_2 is an indirect allowed transition, i.e., n = 2. As a result, Tauc plot can be obtained by plotting hυ on X-axis and $(\alpha h\upsilon)^{1/n}$ on Y-axis and by extrapolation [50] as highlighted in Fig. 2a, and b.

The energy bandgaps for CTO-4, CTO-8, CTO-12, and CTO-16 samples were 2.56, 1.88, 2.03, and 2.08 eV with variation in the Cu concentration from 4 to 16 wt.%, respectively. From the results, one can conclude that the bandgap of CTO samples initially decreases with an increase in dopant concentration up to 8 wt.%, bandgap increases with an increase in Cu concentration. The minimum bandgap energy observed was 1.88 eV for CTO-8 sample. The obtained results on the bandgap are very much in accordance with Navas et al. group [51].

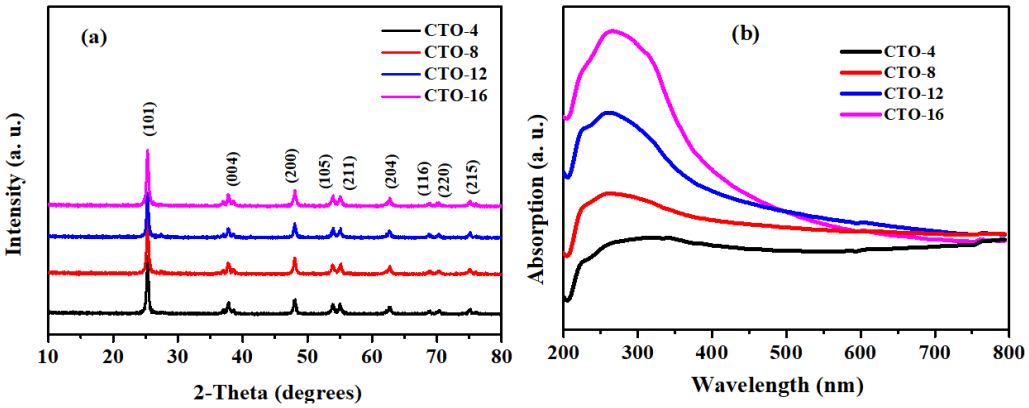

Figure 1. XRD patterns (a), and UV-Vis absorbance spectra (b) of CTO samples.

Table 1. XRD parameters with respect to variation in Cu concentration in TiO_2.

Sample code	Doping concentration (wt.%)	2θ (degrees)	FWHM	Average crystallite (nm)	Microstrain (%)
CTO-4	4	25.319	0.35121	23.18	0.3909
CTO-8	8	25.322	0.33517	24.29	0.3730
CTO-12	12	25.324	0.36743	22.16	0.4088
CTO-16	16	25.324	0.34184	23.82	0.3804

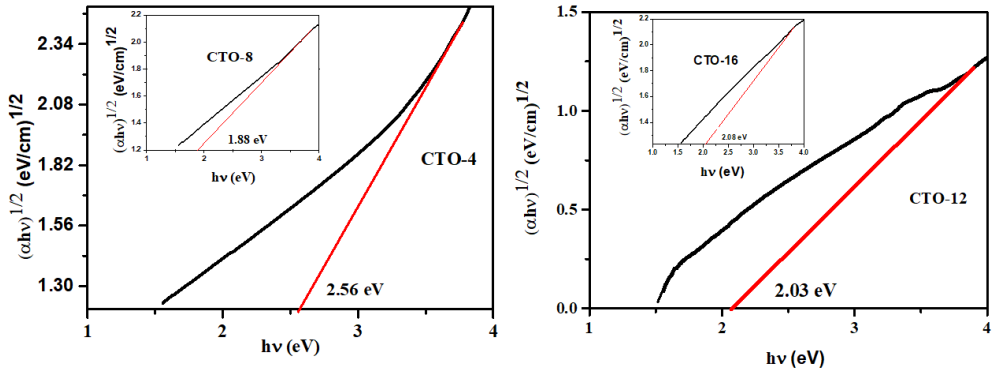

Figure 2. Tauc plots of CTO-4 and CTO-8 (inset) (a), and CTO-12 and CTO-4 (inset) (b).

Bandgap results obtained via density of states (DOS), projected density of states (PDOS), and the electron localization function (ELF) indicated a decrease in bandgap energy from 2.1 to 1.6 eV with Cu doping concentration in anatase TiO_2 NPs increased from 2.5 to 7.5% (as shown in Fig. 3). This narrowing of the bandgap was attributed to the formation of oxygen vacancies and distortion in the anatase structure of TiO_2.

CTO samples showed spherical morphology with an increase in Cu doping and a decrease in the crystallite size. Figure 4a,b represents the SEM micrograph obtained for CTO-8 and CTO-12 samples, respectively. The images clearly show the formation of bigger size particles for CTO-8 as compared to CTO-12. The insets represent the EDS spectra obtained for the corresponding samples, which confirm Ti, O, and Cu's presence. No other signal due to any other impurity indicates the formation of pure Cu-doped TiO_2 NPs. The EDS results revealed the Cu amount in CTO samples as CTO-4:1.85 wt.%, CTO-8:2.45 wt.%, CTO-12:8.82 wt.%, and CTO-16:11.9 wt.%.

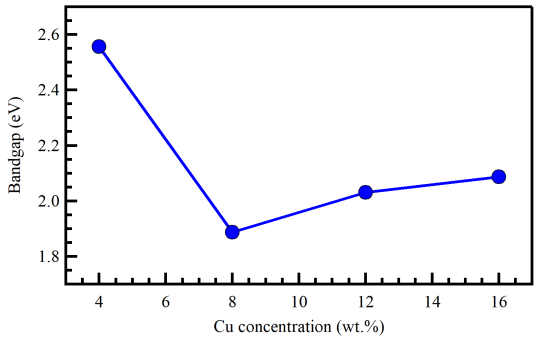

Figure 3. Energy bandgap as functions of copper concentration in TiO_2.

The average particle size estimated from the SEM micrograph is depicted in the histogram plotted (Fig. 4c,d). The obtained values were slightly higher than XRD, i.e., for CTO-8 and CTO-12 samples were 33.98 and 28.74 nm,

respectively. Thus, SEM and XRD data are in good agreement with the particle size.

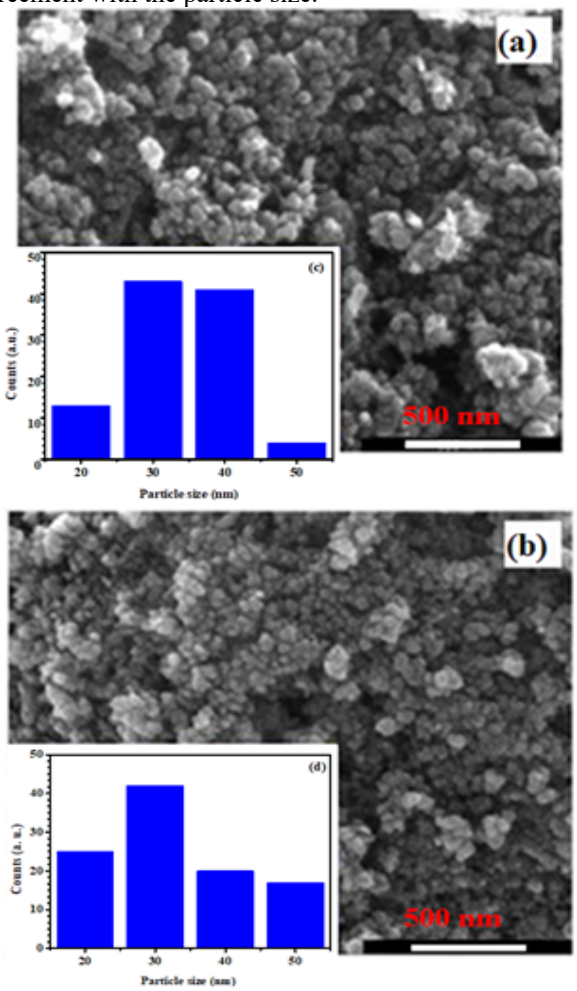

Figure 4. SEM images CTO-8 (a), and CTO-12 (b): and particle size distribution of CTO-8 (c), and CTO-12 (d) samples.

Figure 5 illustrates the room temperature PL spectra recorded for CTO-4 to CTO-16, exhibiting two prominent peaks in the PL spectra. The first broad peak appears between 325–425 nm, with the peak centered at 373.64 nm, while the second sharp and narrow peak is observed at 463.84 nm. The first peak is due to the near band edge emission (NBE) in TiO_2, and the second peak can be attributed to the blue or deep-level emission (DLE) in Cu-doped TiO_2 NPs arising due to oxygen vacancies leading to crystal defects. Interestingly increment in the Cu concentration causes a systematic decrease in the PL intensity. Moreover, when NBE to DLE intensity is compared, it clearly shows a reduction in the PL intensity, indicating a lower recombination rate of electron-hole pairs and higher separation efficiency. This can be attributed to the electron transfer processes from the excited state (conduction band) to the new levels introduced by the Cu metal dopants. The result matches the already reported PL results of Cu-doped TiO_2 NPs, where Cu doping causes a reduction in PL intensity when compared to undoped TiO_2. Karunakaran et al.'s work on Cu-doped TiO_2 NPs also showed NBE and DLE peaks centered at 418 nm and 485 nm in their PL spectra [52]. In this case, the blue shift in the peak position may be due to the smaller size and pure anatase phase of the Cu-doped TiO_2 NPs prepared by the sol-gel method. In contrast, the Karunakaran group utilized the modified ammonia-evaporation-induced method to prepare mixed-phase (anatase+rutile) Cu-doped TiO_2 NPs.

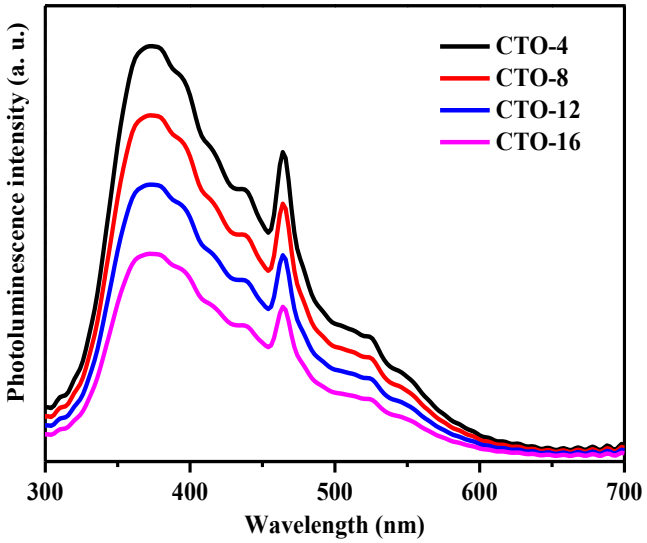

Figure 5. Photoluminescence spectra obtained for CTO samples.

In photodegradation tests, the CTO catalyst's dependence on the photodegradation efficiency indicated an increase in the degradation percentage with an increase in the amount of catalyst from 0.1 g/L. It reaches the highest value for 0.2 g/L, and with a further increase in the catalyst (0.3 g/L), the degradation efficiency is reduced. This could be understood based on the penetration depth of UV, scattering effect, and active sites available on the catalyst surface [53]. From the preliminary experiments, one could conclude that the CTO-12 sample with 12 wt.% of Cu showed the best performance. This could be attributed to its small size (22.16 nm), which will possess a higher surface area according to the quantum confinement effect. Hence, CTO-12 served as a nanocatalyst and was tested for photocatalytic degradation of dyes. The evolution of the optical absorption spectra of MB dye solution with and without catalysts as a function of irradiation time is shown in Fig. 6.

The characteristic absorbance of MB dye was observed at 664 nm in both cases. Zhang et al. also reported the characteristic absorbance peak of MB aqueous dye solution at the same position [27]. The spectra indicate the continuous and fast MB decomposition of dye in the presence of CTO-12.

The absorption spectra for subsequent photodegradation of RhB and MO dyes in the presence and absence of CTO-12 catalyst are depicted in Fig. 7 and Fig. 8, respectively. The obtained absorption spectra indicate the improved degradation of dyes in the presence of CTO-12 catalyst compared to only dye. The characteristic absorbance peaks of RhB and MO dyes were seen at 553 and 464 nm, respectively, which agrees with the reported characteristic peaks of dyes [34, 54].

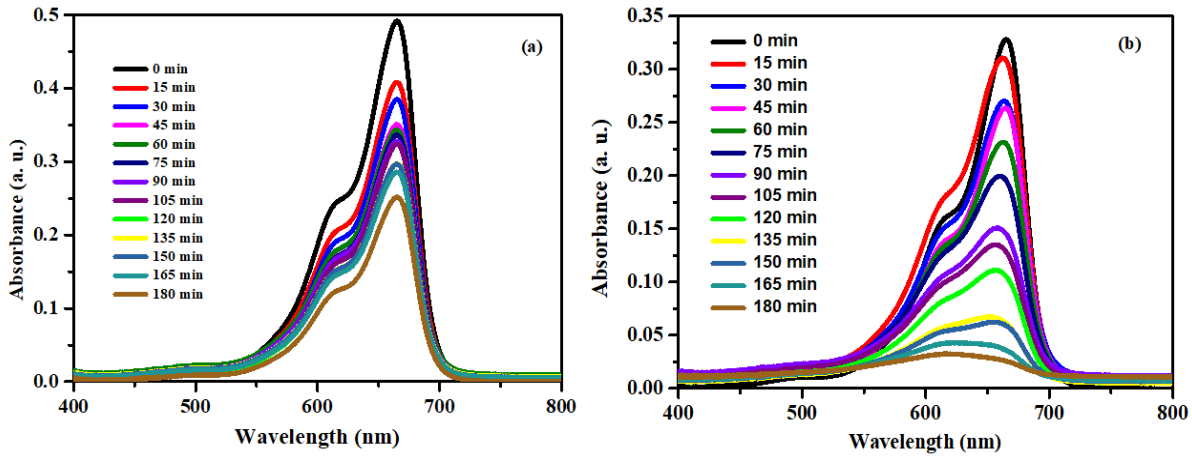

Figure 6. Absorbance spectra of MB dye: without (a), and with catalysts (b).

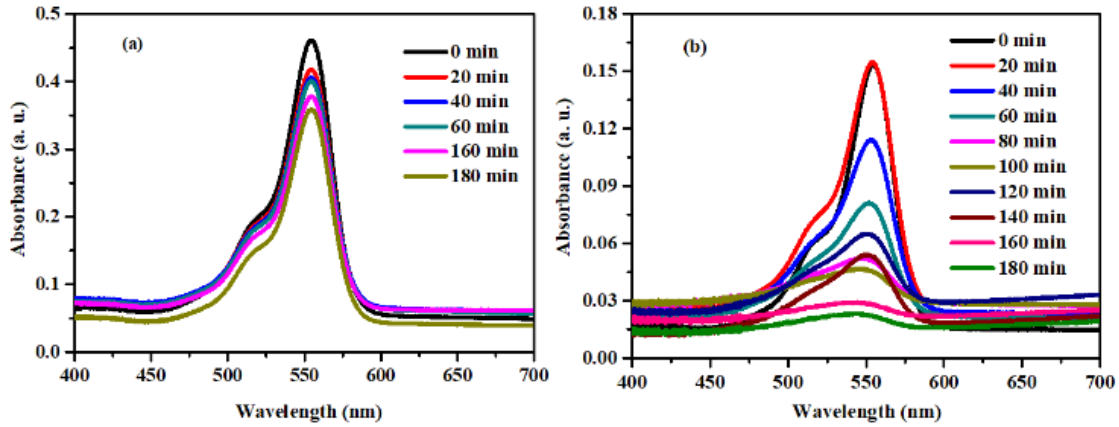

Figure 7. Absorbance spectra of RhB dye: without (a), and with catalysts (b).

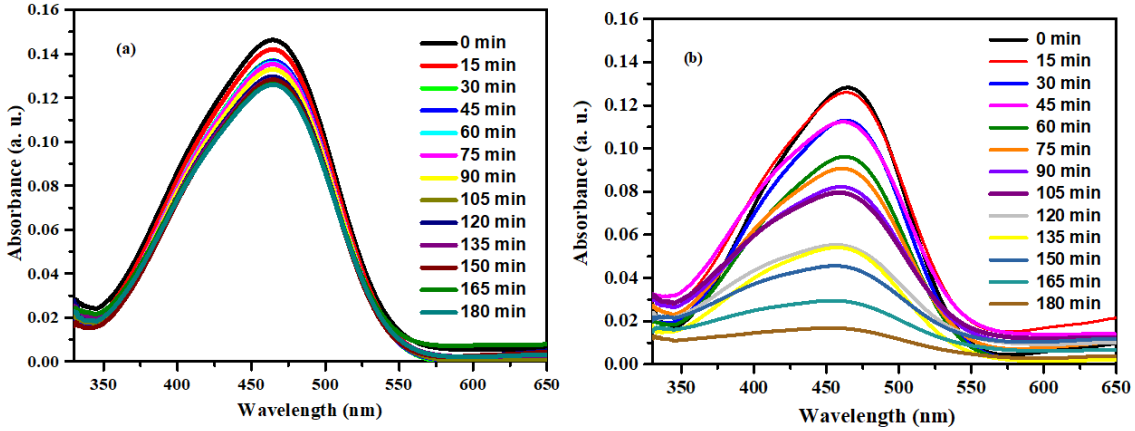

Figure 8. Absorbance spectra of MO dye: without (a), and with catalysts (b).

Figure 9 illustrates the photodegradation of MB, MO, and RhB dyes subjected to UV-light irradiation for 180 min. The insets of the figure illustrate the decolorization of the various cationic and anionic dyes. The photodegradation percentage for all the dyes considered was estimated by using Eq. (1). The data reveal that MB dye's photocatalytic removal efficiency with CTO-12 catalyst reaches about 91.93% at 180 min of irradiation, while only 48.76% of removal efficiency is observed without CTO-12 catalyst.

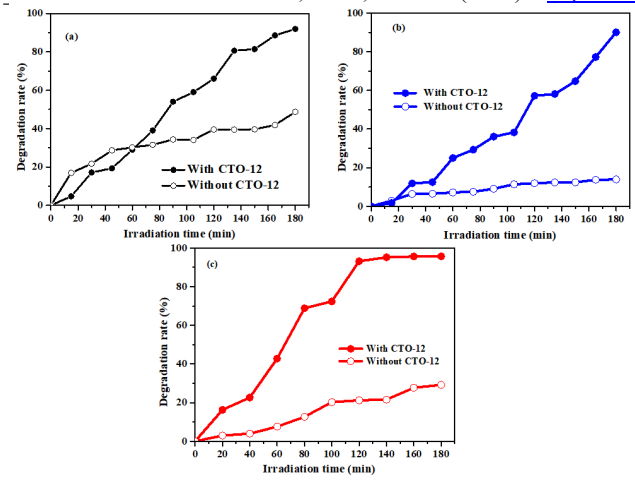

Figure 9. Degradation percentage as a function of irradiation time: Methylene blue (a), Methyl orange (b), and Rhodamine B (c). Insets show corresponding dye decolorization.

According to literature, Aguilar et al. reported about 90% of MB degradation at 480 min for 5% Cu-doped TiO_2 NPs [19], while 80% photodegradation at 300 min was observed by Zhang et al. for Cu-doped TiO_2 thin films under visible light irradiation [27]. The estimated photodegradation percentage of RhB dye was about 95.58% in the presence of CTO-12 catalyst, which is 3.5-times higher than the degradation in the absence of the catalyst (27.17%) at 180 min irradiation of UV light. In the case of MO dye, the value observed was 89.12%. This value was more than 6-times higher when compared with only MO dye (13.91%).

To perform a comparative photodegradation study between cationic and anionic dyes using CTO under UV light, the histogram plot was done, which is shown in Fig. 10. The plot clearly demonstrates that irrespective of cationic or anionic dye in all the cases, the degradation was higher when CTO was used. Moreover, the maximum degradation was observed for the cationic dye (RhB) and the minimum for the anionic dye (MO). The degradation efficiency was found in the order of RhB>MB>MO.

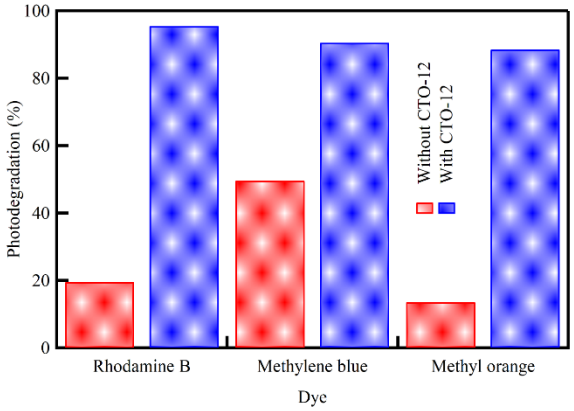

Figure 10. Histogram for the comparative activity of organic dyes without (W/O-C) and with (W-C) CTO-12 catalyst.

Further absorption and degradation data obtained emphasize that the CTO-12 (12 wt.% Cu-TiO_2 NPs) was efficient in the degradation of RhB, MB, and MO, and it followed the first-order kinetics. Using Eq. (3), the apparent pseudo-first-order rate constant (K_{app}) can be calculated as follows [40, 55, 56]:

$$-\ln\frac{C}{C_o} = K_{app}t \quad (3)$$

The plot of $-\ln(C/C_0)$ versus irradiation time for CTO-12 photocatalyst at different initial dye concentrations (10, 20, and 30 mg/L) is highlighted in Fig. 11. Table 2 describes the apparent rate constant (K_{app}) of MB, RhB, and MO photodegradation reactions over CTO-12 photocatalyst (0.2 g/L). The values were found to be 0.01216, 0.02061, and 0.01858 min^{-1}, respectively. With the increase in the initial dye concentration, the apparent rate constant was found to decrease. Considering the Langmuir-Hinshelwood model, one can attribute this to the quenching effect between excited organic dye molecules at higher dye concentrations when subjected to UV light irradiation [53].

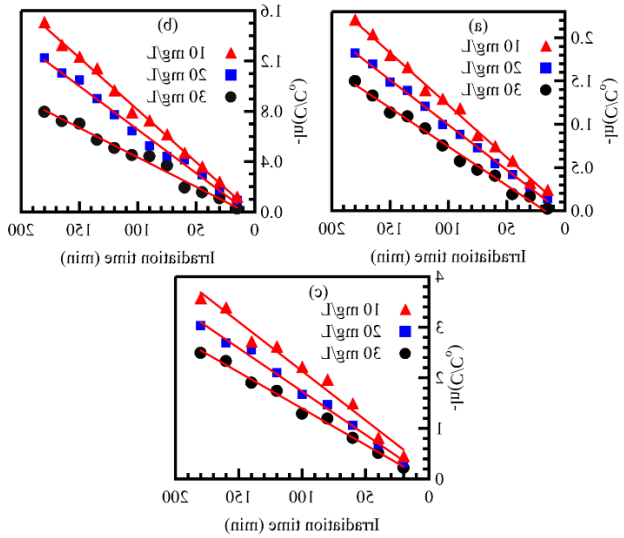

Figure 11. The plot of $-\ln(C/C_o)$ versus irradiation time with CTO-12 catalysts for Methylene blue (a), Methyl orange (b), and Rhodamine B (c).

Table 2. The reaction rate constant of various dye photocatalytic decomposition with variation in initial dye concentrations

Dye solutions	Initial concentration (mg/L)	K_{app} (min^{-1})	R^2
MB	10	0.01216	0.9981
MB	15	0.00952	0.9968
MB	20	0.00536	0.9853
Rh-B	10	0.02061	0.9958
Rh-B	15	0.01736	0.9917
Rh-B	20	0.01382	0.9819
MO	10	0.01858	0.9966
MO	15	0.01561	0.9929
MO	20	0.01107	0.9844

Results indicate that the apparent rate constant K_{app} = 0.02061 min^{-1} is the maximum for the RhB dye. This also signifies that the photocatalytic activity of the Cu-doped TiO_2 nanocatalyst is improved concerning their counter dyes [57]. Furthermore, the regression coefficient (R^2) values found were 0.9981, 0.9958, and 0.9966, which implies the

photodegradation of MB, RhB, and MO catalyzed by CTO-12 fit into the Langmuir-Hinshelwood kinetic model [58]. Similar to our results, Kuyumcu et al. also reported the highest apparent rate constants for Cu among the transition metal series (Mn, Fe, Ni, Co) doped TiO_2 photocatalyst under visible light irradiation [23].

The photodegradation of MB dye in the presence of CTO-12 catalyst is illustrated in Fig. 12. In the present study, Cu metal ions create a trapped site that directly affects charge carriers' lifetime. Here the electrons (e^-) present in the Ti are transferred to the conduction band (CB) of Cu (metal sites), which act as traps for generated e^-, improving the probability of photoreaction between e^- and holes (h^+) pairs and reactive O_2 species by increasing the lifetime of charge carriers [23]. The electron-hole pairs migrate onto the surface of Cu/TiO_2, where the organic dye molecules are absorbed. The holes in the valance band (VB) undergo a reaction with water (H_2O) and hydroxide ions (OH^-); as a result, hydroxyl radicals ($OH^\bullet$) and protons (H^+) can be formed.

Similarly, electrons in the CB accumulate on the Cu that reacts with O_2 to form superoxide ions ($O_2^{\bullet-}$). Superoxide ions usually have an excellent reducing ability when they react with a proton, generating hydroperoxyl radical ($HO_2^\bullet$). These radicals react with organic dye molecules, which was adsorbed on surfaces of catalyst CTO-12. Finally, the effluent, organic dye molecules will be converted into carbon dioxide (CO_2) and H_2O at the end of sequential oxidation-reduction reactions [33]. The same mechanism is also valid for the other two dyes used in this work. Similar to MB's case, scavengers ($OH^\bullet$ and $O_2^{\bullet-}$) react with MO and RhB dyes to degrade into CO_2 and H_2O.

Although the photodegradation mechanism is the same for all three dyes considered, the observed degradation efficiency is different for the cationic (MB, RhB) and anionic (MO) dyes. The possible reason which could be responsible is the surface charges present on the photocatalyst, differences in the chemical structure and molecular weight of the organic dyes, in addition, to change in reactivity among the organic dyes and $OH^\bullet$, which may alter the adsorption characteristics and ultimately the degradation rate of photocatalytic reactions [59]. The RhB dye (479.02 g/mol) belongs to the xanthene group and contains one carboxylic group (-COOH) and two tertiary amines (-$N(CH_2CH_3)_2$) groups that can efficiently react with H^+. In MB (373.88 g/mol), a cationic dye like RhB belongs to the thiazine group with polar atoms. Therefore, a higher degradation percentage is observed for RhB than MB. The anionic dye MO is from the monoazo group having a molecular weight of 327.34 g/mol. Azo group (-N=N-) in methyl orange is responsible for reducing photocatalytic degradation [23]. Meanwhile, thiazine structured MB, which includes nitrogen, negatively charged Cl^- ions, positively charged sulfur atoms, and no azo group, leads to a stronger interaction between the MB dye and CTO-12 catalyst than MO dye. According to Pang et al. report [60], in MO molecules, there also exists -SO_3^- which will attach to the photocatalyst through bidentate coordination via two sulfonic oxygen. As a result, the numerous surface sites become temporarily passivated, which leads to the deactivation of the catalysts. Therefore CTO-12 sample has a higher degradation for MB (91.93 %) than MO (89.12%) dye. The observed photocatalytic degradation order in the presence of CTO-12 follows RhB>MB>MO. Comparison of reported literature with the present work is illustrated in Table 3.

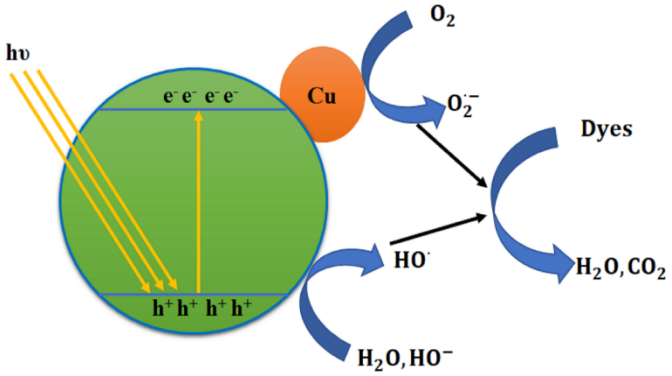

Figure 12. Schematic illustration of the mechanism of photocatalytic degradation of MB dye on CTO-12 photocatalyst under UV light irradiation.

To date, no report is available on the recycling experiments to probe the stability of Cu-doped TiO_2 NPs. Only for thin-film Cu-doped TiO_2 nanotubes arrays as a photocatalyst is reported [26]. MB dye under visible light was used, and catalytic activity was similar at the end of five cycles. Therefore, attempts were made in this direction of recycling testing of CTO-12 for three successive runs. After each run, the photocatalyst was subjected to centrifugation, washing, and drying and then reused for subsequent degradation. The results obtained are depicted in Fig. 13, which indicates the removal rate of RhB, MB, and MO decreased from 95.8, 91.93, and 89.12% to 90.3, 83.9, and 62%, respectively. During the recycling process, the photocatalytic activity of CTO-12 decreases minimally for the cationic dyes compared to anionic dyes, which clearly illustrates the efficiency and high stability of CTO photocatalyst.

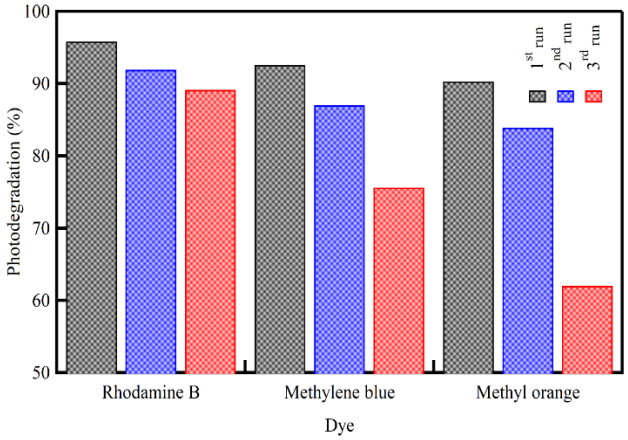

Figure 13. Recycled photoactivity testing of CTO-12 for organic dye degradation for three runs.

Table 3. Comparison of reported photodegradation works on Cu-doped TiO_2 system with the present work

Catalyst	Catalyst conc. (g/L)	Dye	Dye conc. (mg/L)	Light source	Irradiation time (min.)	Degradation ratio (%)	Ref.
Cu-TiO_2 NPs	0.3	MB	56	Visible (High-Efficiency White LED's)	480	90.00	[19]
TiO_2-Cu/PTh (P1-100, 0.75, 0.5; P2- 100, 0.75, 1; P3- 100, 0.75, 2) nanohybrid NPs	0.05–0.25	RhB	2-10	Visible (400 W, Mercury vapor lamp with UV filter)	---	P2 - highest	[34]
TiO_2 NP, TiO_2 HS, Cu_2O/TiO_2 NP, Cu_2O/TiO_2 Hetero structured hollow spheres	0.5	RhB	5	Solar light (300 W, Xe lamp); (420 nm cut off filter were used) Visible light	120 300	Cu_2O/TiO_2 HS highest	[54]
Cu-TiO_2 Nanotube arrays (Thin film)	Electrodes (Bare TiO_2, 1% Cu TiO_2, 3% $CuTiO_2$)	MB	2	Visible (200 W, Xe lamp and 420 nm cut off filter)	120	1% $CuTiO_2$ >3% $CuTiO_2$> TiO_2 nanotube arrays.	[27]
0.3% M/TiO_2 (M=Cu, Ni, Co, Fe, Mn, and Cr) NPs	1	MB MO	5	Visible (105 W, white fluorescent lamp with emission of 530 nm)	300	81.0 44.05	[23]
Cu_2O-CuO/ TiO_2 NPs	0.025-0.15	Reactive Blue 49,	5-25	UV irradiation (30 W, at λ = 365 nm)	80	84.00	[61]

		Reactive Red 24, and Reactive Yellow 160					
Cu-ZnO/TiO_2	0.3-0.7	MB and MO	20-50	Visible (14-23 W, fluorescent lamp)	40-120	77.15 78.45	[35]
TiO_2 and Cu-TiO_2 (0.1, 0.2, 0.3, 2, 4, 6, 8 and 10 mol.%)	---	MB	7.99	UV light irradiation	180	16.00	[26]
Bimetallic Cu-Ni/TiO_2; 10 wt%-9Cu:1Ni-200; 10 wt.% 9Cu:1Ni-180 NPs	1	Orange II	50	Visible (500 W, halogen lamp)	60	89.9 (9Cu:1Ni-200); 83 (9Cu:1Ni-180)	[37]
Cu@C,N,S –TiO_2 and Co@C,N,S –TiO_2	1	MO	10	UV and Visible (500 W, Xe lamp)	60; 180	Cu metal basis > Co non-metal basis.	[31]
TiO_2: Cu (98.5:1.5) (Thin Films)	250, 500, 1000 and 2000 nm Thickness	MB	600	Visible LED source (430 W m^{-2})	1440	42.00 for 2000 nm thickness	[62]
Cu-TiO_2 NPs	2	RhB	100	Sunlight	120	97.00	[63]
Raschig ring (RR)@TiO_2-Cu (0.004% - 0.081%)	500	MB	12.79	Solar simulated Hanau Suntest Lamp >800 nm removed by	210		[28]

				IR Filter, <350 nm removed by pyrex wall of reaction vessels (90 mW cm^{-2})			
TiO_2, 3%Cu-TiO_2, 3%Ag-TiO_2, 3%Eu-TiO_2	9.98	MB	6.39	Visible (200 W, Xenon lamp)	120	3.00 (Ag-TiO_2 Improved degradation)	[24]
(Cu, N) - codoped TiO_2, Cu-doped TiO_2, N-doped TiO_2, TiO_2 NPs	0.1	MO	9.81 3.19	UV (30 W, Mercury lamp) and Visible (500 W, Xe lamp with 400 nm glass filter to block UV light)	360	92.00 Cu,N Codoped TiO_2>N-TiO_2>Cu-TiO_2>TiO_2	[29]
Cu-TiO_2/ZnO NPs	1	MO	15	Visible (500 W, Xe lamp with 420 nm cut off filter)	60	83.00 (3% Cu-TiO_2/30% ZnO)> 61.00 (3% Cu-TiO_2)	[36]
Cu-doped TiO_2 NPs	0.2	MB, MO, RhB	10	UV light (64 W, Mercury lamp)	180	91.93, 89.12 and 95.58 %	Present work

4 Conclusions

In summary, highly efficient Cu-doped TiO_2 (CTO) photocatalysts were synthesized using the sol-gel technique. The optical absorption study showed a single broad peak observed between 260-320 nm obtained for various CTO samples. XRD exhibited a pure anatase phase with the smallest particle size obtained for 12 wt.% Cu (CTO-12). In addition, with an increase in the Cu concentration (4 to 16 wt.%), the particle size was first found to decrease and then increase. SEM results demonstrated spherical morphology while AAS and EDS technique confirmed the Cu dopant in CTO samples. From Tauc plot, the bandgaps were observed to be 2.56, 1.88, 2.03, and 2.08 eV for CTO-4, CTO-8, CTO-12, and CTO-16 samples, respectively. The room temperature PL spectra exhibited two prominent peaks, which could be attributed to the near band edge emission and blue or deep level emission arising due to oxygen vacancies leading to crystal defects. Selected CTO-12 photocatalyst demonstrated high photocatalytic activity for cationic dyes (RhB, 95.8%; MB, 91.93%) than anionic dyes (MO, 89.12%). The recyclability experiment performed showed the high stability of CTO-12. It has demonstrated that without surface modifications, complex co-doping processes, or nanocomposite formation CTO photocatalyst

is highly efficient, low-cost, and eco-friendly for effectively treating organic dye wastewater.

Acknowledgement

This work was supported by RGEMS project, VIT-AP/2018/VC/RGEMS/4, VIT-AP University, Amaravati, Andhra Pradesh, India. In addition, A.V. Soldatov acknowledges the financial support from the Ministry of Science and Higher Education of the Russian Federation (State assignment in the field of scientific activity, № 0852-2020-0019.

References

[1] A.H. Jawad, N.S.A. Mubarak, M.A.M. Ishak, K. Ismail, W.I. Nawawi, Kinetics of photocatalytic decolourization of cationic dye using porous TiO_2 film, *Journal of Taibah University for Science,* **10(3)** 352-362, 2016.

[2] C. Luo, X. Ren, Z. Dai, Y. Zhang, X. Qi, C. Pan, Present perspectives of advanced characterization techniques in TiO_2-based photocatalysts, *ACS Appl. Mater. Interfaces,* **9(28)** 23265-23286, 2017.

[3] J. Singh, N. Tripathi, S. Mohapatra, Synthesis of Ag–TiO_2 hybrid nanoparticles with enhanced photocatalytic activity by a facile wet chemical method, *Nano-Structures & Nano-Objects,* **18** 100266-100273, 2019.

[4] H.R. Pouretedal, A.M. Sohrabi, Photosensitization of TiO_2 by ZnS and bromo thymol blue and its application in photodegradation of para-nitrophenol, *Journal of the Iranian Chemical Society,* **13(1)** 73-79, 2016.

[5] A. Ajmal, I. Majeed, R.N. Malik, H. Idriss, M.A. Nadeem, Principles and mechanisms of photocatalytic dye degradation on TiO_2 based photocatalysts: a comparative overview, *RSC Advances,* **4(70)** 37003-37026, 2014.

[6] T. Wang, J. Wei, H. Shi, M. Zhou, Y. Zhang, Q. Chen, Z. Zhang, Preparation of electrospun Ag/TiO_2 nanotubes with enhanced photocatalytic activity based on water/oil phase separation, *Physica E: Low-dimensional Systems and Nanostructures,* **86** 103-110, 2017.

[7] A. Di Paola, M. Bellardita, L. Palmisano, Brookite, the least known TiO_2 photocatalyst, *Catalysts,* **3(1)** 36-73, 2013.

[8] M. Landmann, E. Rauls, W.G. Schmidt, The electronic structure and optical response of rutile, anatase and brookite TiO_2, *Journal of Physics: Condensed Matter,* **24(19)** 195503-195508, 2012.

[9] M. Sahu, P. Biswas, Single-step processing of copper-doped titania nanomaterials in a flame aerosol reactor, *Nanoscale Research Letters,* **6** 441-454, 2011.

[10] B. Choudhury, M. Dey, A. Choudhury, Defect generation, d-d transition, and band gap reduction in Cu-doped TiO_2 nanoparticles, *International Nano Letters,* **3(1)** 1-8, 2013.

[11] H.M. Yadav, S.V. Otari, V.B. Koli, S.S. Mali, C.K. Hong, S.H. Pawar, S.D. Delekar, Preparation and characterization of copper-doped anatase TiO_2 nanoparticles with visible light photocatalytic antibacterial activity, *Journal of Photochemistry and Photobiology A: Chemistry,* **280** 32-38, 2014.

[12] J. Lee, S.L. Bartelt-Hunt, Y. Li, E.J. Gilrein, The influence of ionic strength and organic compounds on nanoparticle TiO_2 (n-TiO_2) aggregation, *Chemosphere,* **154** 187-193, 2016.

[13] T.L. Palma, B. Vieira, J. Nunes, J.P. Lourenço, O.C. Monteiro, M.C. Costa, Photodegradation of chloramphenicol and paracetamol using PbS/TiO_2 nanocomposites produced by green synthesis, *Journal of the Iranian Chemical Society,* **17(8)** 2013-2031, 2020.

[14] S.A. Ansari, M.M. Khan, M.O. Ansari, M.H. Cho, Nitrogen-doped titanium dioxide (N-doped TiO_2) for visible light photocatalysis, *New Journal of Chemistry,* **40(4)** 3000-3009, 2016.

[15] Z. Fan, F. Meng, J. Gong, H. Li, Z. Ding, B. Ding, One-step hydrothermal synthesis of mesoporous Ce-doped anatase TiO_2 nanoparticles with enhanced photocatalytic activity, *Journal of Materials Science: Materials in Electronics,* **27(11)** 11866-11872, 2016.

[16] J.B. Varley, A. Janotti, C.G. Van de Walle, Mechanism of visible-light photocatalysis in nitrogen-doped TiO2, *Adv. Mater. (Weinheim, Ger.),* **23(20)** 2343-2347, 2011.

[17] J. Chebwogen, O. Munyati, S. Hatwaambo, M. Mwamburi, C. Maghanga, Fabrication and characterization of cobalt pigmented anodized zinc for photocatalytic application, *International Journal of Thin Film Science and Technology,* **9(2)** 127-132, 2020.

[18] R.K. Dutta, Nano structural properties of lead doped cadmium sulfide (Cd1-xPbxS) thin films deposited by spray pyrolysis technique, *International Journal of Thin Film Science and Technology,* **9(1)** 21-25, 2020.

[19] T. Aguilar, J. Navas, R. Alcántara, C. Fernández-Lorenzo, J.J. Gallardo, G. Blanco, J. Martín-Calleja, A route for the synthesis of Cu-doped TiO_2 nanoparticles with a very low band gap, *Chemical Physics Letters,* **571** 49-53, 2013.

[20] B. Rajamannan, S. Mugundan, G. Viruthagiri, P. Praveen, N. Shanmugam, Linear and nonlinear optical studies of bare and copper doped TiO_2 nanoparticles via sol gel technique, *Spectrochimica Acta Part A: Molecular and Biomolecular Spectroscopy,* **118** 651-656, 2014.

[21] B. Bharati, A. Sonkar, N. Singh, D. Dash, C. Rath, Enhanced photocatalytic degradation of dyes under sunlight using biocompatible TiO_2 nanoparticles, *Materials Research Express,* **4(8)** 085503, 2017.

[22] G. Song, C. Luo, Q. Fu, C. Pan, Hydrothermal synthesis of the novel rutile-mixed anatase TiO_2 nanosheets with dominant {001} facets for high photocatalytic activity,

RSC Advances, **6(87)** 84035-84041, 2016.

[23] Ö. Kerkez-Kuyumcu, E. Kibar, K. Dayıoğlu, F. Gedik, A.N. Akın, Ş. Özkara-Aydınoğlu, A comparative study for removal of different dyes over M/TiO_2 (M= Cu, Ni, Co, Fe, Mn and Cr) photocatalysts under visible light irradiation, *Journal of Photochemistry and Photobiology A: Chemistry,* **311** 176-185, 2015.

[24] J.V. Hernández, S. Coste, A.G. Murillo, F.C. Romo, A. Kassiba, Effects of metal doping (Cu, Ag, Eu) on the electronic and optical behavior of nanostructured TiO_2, *Journal of Alloys and Compounds,* **710** 355-363, 2017.

[25] C. Garlisi, G. Scandura, J. Szlachetko, S. Ahmadi, J. Sa, G. Palmisano, E-beam evaporated TiO_2 and Cu-TiO_2 on glass: Performance in the discoloration of methylene blue and 2-propanol oxidation, *Applied Catalysis A: General,* **526** 191-199, 2016.

[26] M.M. Momeni, Y. Ghayeb, Z. Ghonchegi, Fabrication and characterization of copper doped TiO_2 nanotube arrays by in situ electrochemical method as efficient visible-light photocatalyst, *Ceramics International,* **41(7)** 8735-8741, 2015.

[27] W. Zhang, Y. Liu, B. Yu, J. Zhang, W. Liang, Effects of silver substrates on the visible light photocatalytic activities of copper-doped titanium dioxide thin films, *Materials Science in Semiconductor Processing,* **30** 527-534, 2015.

[28] F. Bensouici, M. Bououdina, A. Dakhel, R. Tala-Ighil, M. Tounane, A. Iratni, T. Souier, S. Liu, W. Cai, Optical, structural and photocatalysis properties of Cu-doped TiO_2 thin films, *Applied Surface Science,* **395** 110-116, 2017.

[29] S. Reda, M. Khairy, M. Mousa, Photocatalytic activity of nitrogen and copper doped TiO_2 nanoparticles prepared by microwave-assisted sol-gel process, *Arabian Journal of Chemistry,* doi.org/10.1016/j.arabjc.2017.02.002, 2017.

[30] K.C. Christoforidis, M. Fernández-García, Photoactivity and charge trapping sites in copper and vanadium doped anatase TiO_2 nano-materials, *Catalysis Science & Technology,* **6(4)** 1094-1105, 2016.

[31] M. Hamadanian, S. Karimzadeh, V. Jabbari, D. Villagrán, Synthesis of cysteine, cobalt and copper-doped TiO_2 nanophotocatalysts with excellent visible-light-induced photocatalytic activity, *Materials Science in Semiconductor Processing,* **41** 168-176, 2016.

[32] F. Tian, Z. Wu, Y. Yan, B.-C. Ye, D. Liu, Synthesis of visible-light-responsive Cu and N-codoped AC/TiO_2 photocatalyst through microwave irradiation, *Nanoscale Research Letters,* **11(1)** 292-301, 2016.

[33] M.-C. Wu, P.-Y. Wu, T.-H. Lin, T.-F. Lin, Photocatalytic performance of Cu-doped TiO_2 nanofibers treated by the hydrothermal synthesis and air-thermal treatment, *Applied Surface Science,* **430** 390-398, 2018.

[34] M.R. Chandra, T.S. Rao, S. Pammi, B. Sreedhar, An enhanced visible light active rutile titania–copper/polythiophene nanohybrid material for the degradation of rhodamine B dye, *Materials Science in Semiconductor Processing,* **30** 672-681, 2015.

[35] M.R.D. Khaki, B. Sajjadi, A.A.A. Raman, W.M.A.W. Daud, S. Shmshirband, Sensitivity analysis of the photoactivity of Cu–TiO_2/ZnO during advanced oxidation reaction by adaptive Neuro-Fuzzy selection technique, *Measurement,* **77** 155-174, 2016.

[36] M. Dorraj, M. Alizadeh, N.A. Sairi, W.J. Basirun, B.T. Goh, P.M. Woi, Y. Alias, Enhanced visible light photocatalytic activity of copper-doped titanium oxide–zinc oxide heterojunction for methyl orange degradation, *Applied Surface Science,* **414** 251-261, 2017.

[37] N. Riaz, F. Chong, Z. Man, R. Sarwar, U. Farooq, A. Khan, M. Khan, Preparation, characterization and application of Cu–Ni/TiO_2 in Orange II photodegradation under visible light: effect of different reaction parameters and optimization, *RSC Advances,* **6(60)** 55650-55665, 2016.

[38] M. Giahi, D. Pathania, S. Agarwal, G.A.M. Ali, K.F. Chong, V.K. Gupta, Preparation of Mg-doped TiO_2 nanoparticles for photocatalytic degradation of some organic pollutants, *Studia Universitatis Babes-Bolyai, Chemia,* **64(1)** 7-18, 2019.

[39] M. Madhukara Naik, H.S. Bhojya Naik, G. Nagaraju, M. Vinuth, K. Vinu, R. Viswanath, Green synthesis of zinc doped cobalt ferrite nanoparticles: Structural, optical, photocatalytic and antibacterial studies, *Nano-Structures & Nano-Objects,* **19** 100322-100334, 2019.

[40] A.S. Ethiraj, P. Uttam, V. K, K.F. Chong, G.A.M. Ali, Photocatalytic performance of a novel semiconductor nanocatalyst: Copper doped nickel oxide for phenol degradation, *Materials Chemistry and Physics,* **242** 122520, 2020.

[41] M. Solehudin, U. Sirimahachai, G.A.M. Ali, K.F. Chong, S. Wongnawa, One-pot synthesis of isotype heterojunction g-C_3N_4-MU photocatalyst for effective tetracycline hydrochloride antibiotic and reactive orange 16 dye removal, *Advanced Powder Technology,* **31(5)** 1891-1902, 2020.

[42] D. Anbuselvan, S. Muthukumaran, Defect related microstructure, optical and photoluminescence behaviour of Ni, Cu co-doped ZnO nanoparticles by co-precipitation method, *Optical Materials,* **42** 124-131, 2015.

[43] A.A.A. El-Rady, M.S.A. El-Sadek, M.M.E.-S. Breky, F.H. Assaf, Characterization and photocatalytic efficiency of palladium doped-TiO_2 nanoparticles, *Advances in Nanoparticles,* **2(04)** 372-377, 2013.

[44] G.A.M. Ali, O.A. Fouad, S.A. Makhlouf, Structural, optical and electrical properties of sol–gel prepared mesoporous Co_3O_4/SiO_2 nanocomposites, *Journal of Alloys and Compounds,* **579** 606-611, 2013.

[45] E.R. Shaaban, M.Y. Hassaan, G. Moustafa, A. Qasem, G.A.M. Ali, E.S. Yousef, Optical constants, dispersion parameters and non-linearity of different thickness of $As_{40}S_{45}Se_{15}$ thin films for optoelectronic applications, *Optik,* **186** 275-287, 2019.

[46] G.A.M. Ali, O.A. Fouad, S.A. Makhlouf, M.M. Yusoff, K.F. Chong, Optical and Electrochemical Properties of Co_3O_4/SiO_2 Nanocomposite, *Advanced Materials*

Research, **1133** 447-451, 2016.

[47] M. Shahid, I.A. Alsafari, A. Jamil, F.A. Ahmed Ali, S. Haider, P. Agboola, I. Shakir, Dysprosium substituted nickel cobalt ferrite nanomaterials and their composites with reduced graphene oxide for photocatalysis, *Journal of Taibah University for Science,* **14(1)** 1308-1316, 2020.

[48] O. Adedokun, V.M. Odebunmi, Y.K. Sanusi, Effect of annealing temperature on structural, optical and electrical properties of spin coated tin oxide thin films for solar cells application, *International Journal of Thin Film Science and Technology,* **8(3)** 157-162, 2019.

[49] A. Bouafia, S.E. Laouini, M.L. Tedjani, G.A.M. Ali, A. Barhoum, Green biosynthesis and physicochemical characterization of Fe_3O_4 nanoparticles using Punica granatum L. fruit peel extract for optoelectronic applications, *Text. Res. J.,* 00405175211006671, 2021.

[50] Y. Zhao, C. Li, X. Liu, F. Gu, H. Jiang, W. Shao, L. Zhang, Y. He, Synthesis and optical properties of TiO_2 nanoparticles, *Materials Letters,* **61(1)** 79-83, 2007.

[51] J. Navas, A. Sánchez-Coronilla, T. Aguilar, N.C. Hernández, M. Desireé, J. Sánchez-Márquez, D. Zorrilla, C. Fernández-Lorenzo, R. Alcántara, J. Martín-Calleja, Experimental and theoretical study of the electronic properties of Cu-doped anatase TiO_2, *Physical Chemistry Chemical Physics,* **16(8)** 3835-3845, 2014.

[52] C. Karunakaran, G. Abiramasundari, P. Gomathisankar, G. Manikandan, V. Anandi, Cu-doped TiO_2 nanoparticles for photocatalytic disinfection of bacteria under visible light, *Journal of Colloid and Interface Science,* **352(1)** 68-74, 2010.

[53] C. Chen, J. Liu, P. Liu, B. Yu, Investigation of photocatalytic degradation of methyl orange by using nano-sized ZnO catalysts, *Advances in Chemical Engineering and Science,* **1(01)** 9-14, 2011.

[54] H. Yin, X. Wang, L. Wang, Q. Nie, Y. Zhang, W. Wu, Cu_2O/TiO_2 heterostructured hollow sphere with enhanced visible light photocatalytic activity, *Materials Research Bulletin,* **72** 176-183, 2015.

[55] S. Agarwal, H. Sadegh, Monajjemi Majid, A.S.H. Makhlouf, G.A.M. Ali, A.O.H. Memar, R. Shahryari-ghoshekandi, I. Tyagi, V.K. Gupta, Efficient removal of toxic bromothymol blue and methylene blue from wastewater by polyvinyl alcohol, *Journal of Molecular Liquids,* **218** 191-197, 2016.

[56] H. Sadegh, G.A.M. Ali, A.S.H. Makhlouf, K.F. Chong, N.S. Alharbi, S. Agarwal, V.K. Gupta, MWCNTs-Fe_3O_4 nanocomposite for Hg(II) high adsorption efficiency, *Journal of Molecular Liquids,* **258** 345-353, 2018.

[57] H. Oudghiri-Hassani, S. Rakass, F.T. Al Wadaani, K.J. Al-ghamdi, A. Omer, M. Messali, M. Abboudi, Synthesis, characterization and photocatalytic activity of α-Bi_2O_3 nanoparticles, *Journal of Taibah University for Science,* **9(4)** 508-512, 2015.

[58] V. Scuderi, G. Amiard, R. Sanz, S. Boninelli, G. Impellizzeri, V. Privitera, TiO_2 coated CuO nanowire array: Ultrathin p–n heterojunction to modulate cationic/anionic dye photo-degradation in water, *Applied Surface Science,* **416** 885-890, 2017.

[59] S.E. Laouini, A. Bouafia, A.V. Soldatov, H. Algarni, M.L. Tedjani, G.A.M. Ali, A. Barhoum, Green Synthesized of Ag/Ag2O Nanoparticles Using Aqueous Leaves Extracts of Phoenix dactylifera L. and Their Azo Dye Photodegradation, *Membranes,* **11(7)** 468, 2021.

[60] Y.L. Pang, A.Z. Abdullah, Comparative study on the process behavior and reaction kinetics in sonocatalytic degradation of organic dyes by powder and nanotubes TiO_2, *Ultrasonics sonochemistry,* **19(3)** 642-651, 2012.

[61] A. Ajmal, I. Majeed, R. Malik, M. Iqbal, M.A. Nadeem, I. Hussain, S. Yousaf, G. Mustafa, M. Zafar, M.A. Nadeem, Photocatalytic degradation of textile dyes on Cu_2O-CuO/TiO_2 anatase powders, *Journal of Environmental Chemical Engineering,* **4(2)** 2138-2146, 2016.

[62] L. Suárez, Z. Wei, H. Teixidó, R. Sanjinés, M. Bensimon, C. Pulgarín, J. Kiwi, Cu-decorated Raschig-TiO_2 rings inducing MB repetitive discoloration without release of Cu-ions under solar light, *Journal of Environmental Chemical Engineering,* **5(1)** 310-318, 2017.

[63] V. Kavitha, P. Ramesh, D. Geetha, Synthesis of Cu loaded TiO_2 nanoparticles for the improved photocatalytic degradation of rhodamine B, *International Journal of Nanoscience,* **15(5-6)** 1660002-1660009, 2016.